Chaos, Solitons and Fractals 189 (2024) 115592

Contents lists available at ScienceDirect

Chaos, Solitons and Fractals

journal homepage: www.elsevier.com/locate/chaos

Integrating Virtual and Physical Interactions through higher-order networks to control epidemics

Santiago Lamata-Otín [a,b], Adriana Reyna-Lara [c], Jesús Gómez-Gardeñes [a,b,d,*]

[a] Department of Condensed Matter Physics, University of Zaragoza, Zaragoza, 50009, Aragón, Spain
[b] GOTHAM lab, Institute of Biocomputation and Physics of Complex Systems (BIFI), University of Zaragoza, Zaragoza, 50018, Aragón, Spain
[c] Instituto Tecnológico y de Estudios Superiores de Monterrey, Monterrey, 64849, N.L., Mexico
[d] Center for Computational Social Science, University of Kobe, Kobe, 657-8501, Japan

ARTICLE INFO

Dataset link: https://www.sociopatterns.org/datasets, https://doi.org/10.6084/m9.figshare.7267433, https://figshare.com/articles/dataset/WhatsApp_Data_Set/19785193

Keywords:
Complex networks
Contagion processes
Higher-order interactions

ABSTRACT

In the context of our increasingly digitalized society, virtual interactions have become integral to daily communication, complementing traditional face-to-face interactions. These digital pathways, however, are often overlooked in the context of epidemic control, particularly in Digital Contact Tracing, where adoption rates of tailored wearable applications for this purpose remain suboptimal. This study elucidates the key role of the virtual environment in managing infectious disease outbreaks. We develop an integrated framework that combines various detection strategies to assess the efficacy of virtual tools in bending epidemic waves, analogous to conventional Contact Tracing approaches. Our analysis extends to the dynamics of higher-order interactions — characteristic of virtual platforms — and their contribution to epidemic control. Furthermore, we investigate the interplay between physical and virtual interactions, that aligned interactions optimize epidemic control in daily routine scenarios. Our findings underscore the critical role of virtual interactions in epidemic management, suggesting that current societal structures inherently support innovative detection and control strategies.

1. Introduction

In today's digital age, digital technologies significantly enhance public health responses to infectious diseases by speeding up and refining epidemic control [1,2] through advanced tools and services like awareness campaigns [3] and Contact Tracing applications [4]. Recent research has shown that Digital Contact Tracing can drastically reduce epidemic spread [5–15], particularly through early detection of cases that allows a swift isolation of superspreaders that efficiently alters the epidemic trajectory. However, despite its benefits, Digital Contact Tracing has had limited effectiveness in the context of COVID-19 [13]. In particular, it has been shown that Digital Contact Tracing has prevented less than 10% of cases [14,15] in countries such as Spain, Germany or UK due to a rather low adoption rates of the digital applications that, for instance, only reached the 21% in the case of Spain [16].

Shifting from traditional health-based tracing, in this work we analyze a decentralized approach that leverages social media to enhance detection by empowering individuals to disclose their infectious status. This approach, here termed as *Self-Reported Digital Alert* (SRDA), facilitates a quick and broad communication of exposure — prompting their contacts to seek testing — and potentially overcomes the adoption challenges faced by conventional tracing applications. This latter advantage relies on the use of online social platforms, like WhatsApp, to leverage their vast user base that, in the latter case, has recently reached approximately 2.78 billion active users [17].

Apart from the large coverage of well-established digital communication platforms, their use to disseminate SRDAs offers a distinct advantage: most of the communication channels through social platforms are group-based (61% in the case WhatsApp). Thus, at variance with the pairwise nature of Digital Contact Tracing, modeling the impact of SRDA propagation necessitates considering higher-order interactions among users. The characteristics of higher-order interactions, extensively studied in the field of complex systems [18–20], may significantly affect the onset of collective behaviors as shown in diverse contexts such as percolation [21–23], synchronization [24–27] or social dynamics [28–32]. Thus, in our case, we anticipate that higher-order interactions will be crucial in enhancing the efficacy of SRDAs for controlling epidemic waves.

To show how the propagation of SRDAs through virtual platforms we have followed the following steps. First, in Section 2, we introduce a

* Corresponding author at: Department of Condensed Matter Physics, University of Zaragoza, Zaragoza, 50009, Aragón, Spain.
E-mail address: gardenes@unizar.es (J. Gómez-Gardeñes).

https://doi.org/10.1016/j.chaos.2024.115592
Received 23 May 2024; Received in revised form 24 September 2024; Accepted 26 September 2024
Available online 12 October 2024

general compartmental framework where epidemic spreading competes with three different detection pathways: namely symptomatic detection (SD), Digital Contact Tracing (CT), and those coming from SDRAs in virtual platforms and thus called virtual detection (VD). While the former two (SD and CT) are well-known detection routes acting either at the individual level (SD) or through pairwise interactions (CT), the latter (VD) relies on the structure of higher-order interactions accounting for virtual communication channels. Thereafter, in Section 3 we address the following two questions: *(i)* what does VD add to the well-known SD and CT detection routes? and *(ii)* what is the role of higher-order structures in boosting the effects of VD on epidemic control? Finally, in Section 4, we study epidemic control in realistic scenarios where the physical network and the projection of the virtual structure are not coincident. To this aim, we consider eight face-to-face interaction networks as diffusion spaces for the epidemic. To round off, in Section 5 we draw the main conclusions of our study.

2. Modeling contagion and detection processes

Detection strategies such as Contact Tracing and the proposed Virtual Detection through SRDA propagation can be modeled as a contagion process. In this process, those individuals with the infectious state detected contribute to identifying other positive cases within their social network. This mechanism competes with the direct spread of the virus, thus aiming to curtail its transmission by pinpointing and isolating those actively spreading the infection. It is important to note that the cascade of detections triggered by CT and VD is only activated provided the virus is present in the system and, more importantly, once the first individuals participating in these cascades have tested positive after displaying symptoms.

2.1. Compartmental model

To incorporate the combined detection dynamics into a model for understanding the transmission of SARS-CoV-2, we build an epidemic model with seven states or compartments: Susceptible (S), Exposed (E), Pre-symptomatic (P), Infectious asymptomatic (I_A), Infectious symptomatic (I_S), Detected (D), and Removed (R). The transitions between these states are depicted in Fig. 1 and are explained below. Individuals designated as Susceptible (S) are those who are currently healthy and can potentially become infected. This infection can occur through direct contact with Pre-Symptomatic (P), Asymptomatic (I_A) and Symptomatic (I_S) Infectious agents, being the associated infectivities: β_A, β_A and β_S, respectively. Upon infection, a Susceptible agent transforms into the Exposed (E) state. The Exposed state (E) corresponds to a stage during which an individual exhibits no symptoms and is non-contagious. This state persists for an average duration of η^{-1} days. Following the E state, individuals transition to the Pre-symptomatic state (P). In this stage, no symptoms are apparent, but the individual is already contagious, with a contagion rate denoted as β_A. In the absence of detection, individuals remain in this P state for an average period of α^{-1} days. Following the Pre-symptomatic stage, a fraction $(1-p)$ individuals may persist as asymptomatic (I_A). Those in the I_A compartment share similar characteristics in terms of infectivity and detectability as those in the P stage. In the absence of detection, individuals in this compartment remain, on average, for μ^{-1} days before transitioning to the Removed state (R). Conversely, the remaining fraction (p) of individuals from the P stage proceed to become Infectious symptomatic (I_S). This compartment is distinguished by the infectivity denoted as β_S when coming into contact with an S agent. Similar to the I_A compartment, individuals in the I_S compartment spend an average of μ^{-1} days before progressing to the Removed state (R), unless detected before this transition occurs.

Central to our study is the dynamics around the Detection compartment (D). This stage is accessible to individuals in the P, I_S, and I_A states and, as described in the introductory part, agents in these latter compartments can be detected through three different pathways:

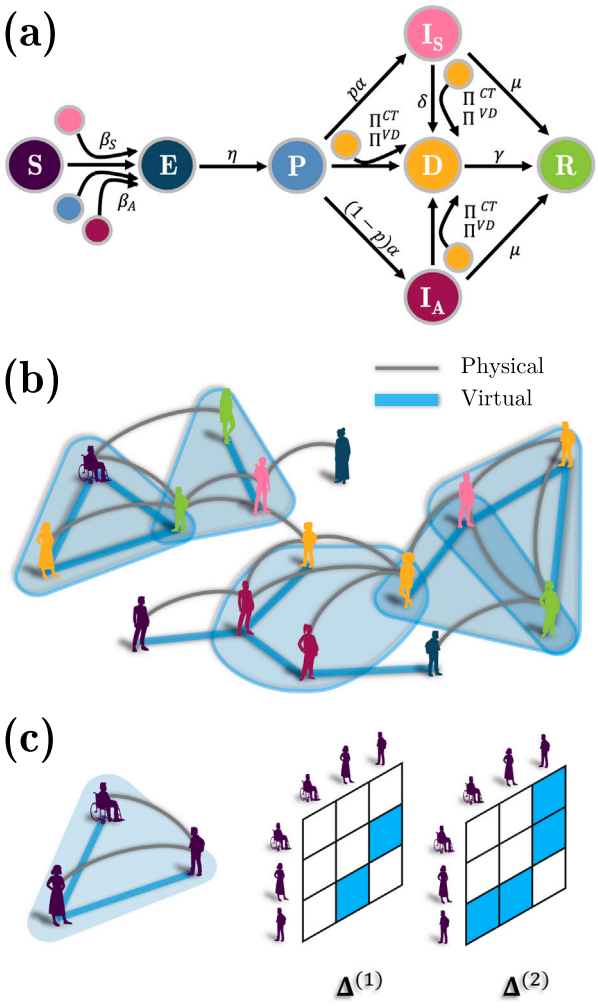

Fig. 1. Compartmental model and interaction channels in spreading and detection dynamics. (a) Spreading and detection compartmental model is described. The model has seven compartments: susceptible (S), exposed (E), presymptomatic (P), infectious asymptomatic (I_A), infectious symptomatic (I_S), detected (D), and recovered (R). Arrows indicate the possible transitions between different states. (b) Types of interactions between individuals: pairwise physical interactions (gray lines) and higher-order virtual interactions (light-blue structures). (c) Schematic representation of the set of matrices $\{\boldsymbol{\Delta}^{(1)},\dots,\boldsymbol{\Delta}^{(M)}\}$ embodying the correlations between the two interaction pathways for each order of interaction (m). In particular, $\Delta^{(1)}_{ij}=1$ if nodes i and j interact both physically and through a virtual group of order $m=1$, and $\Delta^{(1)}_{ij}=0$ otherwise. Similarly, $\Delta^{(2)}_{ij}=1$ if nodes i and j interact both physically and through a virtual group of order $m=2$, and $\Delta^{(2)}_{ij}=0$ otherwise. (For interpretation of the references to color in this figure legend, the reader is referred to the web version of this article.)

1. Symptomatic Detection (SD). Symptomatic infectious individuals (those in I_S) can be promptly identified as they exhibit symptoms with rate δ, which is related to the average time elapsed from the onset of symptoms to taking a viral test. After the detection of symptomatic agents, the other detection routes are initiated.
2. Contact Tracing Detection (CT). The identification of infectious cases (those in compartments P, I_A, and I_S) can occur through Contact Tracing. In this context, we consider that a fraction f of the population utilizes a detection application. Consequently, an agent can be identified provided that both the detected individual (in D) and the corresponding infectious contact (either in P, I_A, or I_S) are equipped with the tracking application, which happens with probability f^2. Hence, the detection rate Π^{CT}, introduced in Fig. 1(a), depends both on the mutual adoption

Table 1
Collection of epidemiological parameters of the $SEPI_AI_SR$ model whose values are fixed and taken from observations regarding SARS-CoV-2 propagation (see references).

Parameter	Explanation	Value	Reference
η	Rate $E \to P$	$1/2.5$ day^{-1}	[34]
α	Rate $P \to I_A, I_S$	$1/2.5$ day^{-1}	[34]
p	Fraction of Symptomatic	0.65	[35]
μ	Rate $I_A, I_S \to R$	$1/7$ day^{-1}	[36,37]

of the application and on the physical interaction of the agents (which guarantees the recording of the contact).

3. Virtual Detection (VD). In addition to CT, the identification of infectious cases (those in P, I_A, and I_S) can also occur via individuals propagating SRDAs virtually. In our model, SDRAs are released through virtual groups (of arbitrary size) to which the infectious user takes part of, and we term the rate at which infectious (undetected) cases decide to undergo testing following this group interaction channel as Π^{VD}.

Finally, regardless of the compartment of provenance, once in the D state an infectious individual cannot spread the pathogen due to isolation, moving to the final stage R with a rate γ. Let us note that the model assumes that detected individuals remain in isolation and stop spreading the disease. This has been reported to be the case in South Korea during the COVID-19 pandemic [33], where the population showed an unwavering commitment. Nevertheless, the impact of those free-riders who do not follow the sanitary rules can be captured as a factor that reduces the actual detection rates.

According to the former description, the $SEPI_AI_SR$ model comprises six epidemiological parameters (plus two more related to the detection process). The values of four of the six epidemiological parameters are outlined in Table 1 , while the values of the remaining two (the infectivities β_A and β_S) depend on the specific network under analysis. In particular, the values of β_A and β_S are chosen such that, in the absence of detection policies, the final size of the epidemic (the attack rate r^∞) is the same ($r^\infty = 0.9$) for all the networks analyzed.

Lastly, regarding the two parameters that characterize detections, γ and δ, we fix $\gamma = 1$ while we choose a small value, $\delta = 0.05$, for the SD rate that trigger the detection channels related to CT and VD. This low value allows us to analyze the isolated and intertwined effects of CT and VD.

2.2. Interaction backbone mediating contagion and detection processes

As shown in Fig. 1(a) and described in the former section, four different transitions are associated to interactions between agents in the system. Namely: $S \to E$, $P \to D$, $I_S \to D$, and $I_A \to D$.

As usual in network epidemiology, we assume that pairwise interactions are dictated by a graph of N nodes (the amount of individuals) and whose L edges are encoded in an $N \times N$ adjacency matrix, $\mathbf{A} = \{a_{ij}\}$, whose entries $a_{ij} = 1$ when nodes i and j interact, and $a_{ij} = 0$ otherwise. With the help of this matrix we can define the number of pairwise physical interactions (the degree) of a node i as: $k_i = \sum_{j=1}^{N} a_{ij}$. In general, in this manuscript, we will consider face-to-face contact data to construct the network of physical interactions. The characteristics of the real networks considered are summarized in Table 2 and, although some of the datasets have temporal resolution, we restrict our study to their static coarse-graining by setting, for these time-varying data sets, a temporal window of five minutes as the minimum interaction time to define a link in the static version of the graph.

Pairwise physical interactions govern completely the backbone of contagion processes, i.e. the transitions $S \to E$, since these events correspond to physical interactions. This way, a Susceptible node i whose neighbor set contains agents in states P, I_A and I_S can be infected by these individuals with the rates described above. In addition

Table 2
Statistics of real-world physical interaction networks. Number of nodes and average connectivity after processing the data as indicated in the manuscript.

Network	N	k	Reference
Malaui village	84	8	[38]
Hospital	72	10	[39]
Scientific conference	330	5	[40]
French high school	324	9	[41]
Workplace	212	9	[42]
Primary school	242	16	[43]
American high school	784	60	[44]
University	675	101	[45]

to contagion processes, the network encapsulated in $\mathbf{A}$ also dictates those detection processes ($P \to D$, $I_S \to D$, and $I_A \to D$) activated through the CT pathway, since it operates through reconstructing those encounters recorded by the application and, obviously, they correspond to physical interactions.

Differently to CT, those detections made via the VD channel do not operate solely through a complex network of pairwise virtual interactions but, instead, use to take place through groups rather than edges. These groups in which SRDAs are disseminated by infectious (and detected) agents are called hyperedges and, all together, form another interaction backbone termed hypergraph. In the hypergraph the collection of groups can be grouped in different sets according to the number of members they contain. In this way, all the groups of $m+1$ individuals compose the class of hyperedges of order m, with $m \in [1, M]$ (note that $m = 1$ correspond to groups of 2 individuals, i.e. virtual links). As shown in Fig. 1(b) the collection of virtual groups (hyperedges) and that of physical edges coexist in such a way that provide different means of interactions to a particular set of individuals.

In order to illustrate the microscopic mechanisms involved in VD and taking place on the hypergraph structure let us focus, without any loss of generality, on one particular order m and a particular node i. This way, the set $\mathcal{E}_i^{(m)}$ is the collection of all the hyperedges which node i belongs to. The cardinality of $\mathcal{E}_i^{(m)}$ corresponds to the generalized degree of order m of node i, defined as $\kappa_i^{(m)}$, so that $\mathcal{E}_i^{(m)} = \{\sigma_1^{i\,(m)}, \dots, \sigma_{\kappa_i^{(m)}}^{i\,(m)}\}$. Once the set $\mathcal{E}_i^{(m)}$ is defined it is useful to quantify the overlap of each group $\sigma_\alpha^{i\,(m)}$ with the physical contacts of node i which are dictated by the adjacency matrix $\mathbf{A}$. To this aim let us first define, for each order of interaction m, an adjacency tensor $\mathbf{A^{(m)}} = \{a^{(m)}_{i,j_1,\dots,j_m}\}$, whose entries $a^{(m)}_{i,j_1,\dots,j_m} = 1$ in case the set of nodes $\{i, j_1, \dots, j_m\}$ corresponds to any of the groups $\sigma_\alpha^{i\,(m)} \in \mathcal{E}_i^{(m)}$, whereas $a^{(m)}_{i,j_1,\dots,j_m} = 0$ otherwise. Second, we define a matrix $\hat{\mathbf{A}}^{(m)} = \{\hat{a}^{(m)}_{ij_1}\}$ whose elements are $\hat{a}^{(m)}_{ij_1} = \Theta\left(a^{(m)}_{i,j_1\dots,j_m}\right)$, where Θ is the Heaviside function. Therefore, we have $\hat{a}^{(m)}_{ij} = 1$ only when nodes i and j are involved in at least one interaction of order m, whereas $\hat{a}^{(m)}_{ij} = 0$ otherwise. Finally, the pairwise physical connections that are replicated in groups of order m can be captured in a new matrix $\mathbf{\Delta}^{(m)}$ whose elements are $\Delta^{(m)}_{ij} = \hat{a}^{(m)}_{ij} \cdot a_{ij}$ so that $\Delta^{(m)}_{ij} = 1$ when there is both a physical interaction and a virtual interaction of order m between nodes i and j, while $\Delta^{(m)}_{ij} = 0$ otherwise, as illustrated in Fig. 1(c). These projection of group interactions into the backbone of physical edges will play an important role in defining Π^{VD} as we will explain below.

Let us also note that we are assuming undirected virtual interactions, as we consider that in the context of SRDAs dissemination, regardless of the social relevance of the individual who disseminates information about their infectious status, the key factor influencing their impact on the recipient is whether or not there was physical contact between the two individuals.

2.3. Microscopic dynamical equations

The dynamics of the introduced compartmental model can be analyzed through a set of coupled differential equations. To this end,

we consider that the dynamical state of a node i at a time t is characterized by the probabilities of being susceptible ($\rho_i^S(t)$), exposed ($\rho_i^E(t)$), presymptomatic ($\rho_i^P(t)$), infectious asymptomatic ($\rho_i^{I_A}(t)$), infectious symptomatic ($\rho_i^{I_S}(t)$), detected ($\rho_i^D(t)$) and recovered ($\rho_i^R(t)$). The differential equations describing the evolution of these probabilities are written as follows:

$$\dot{\rho}_i^S = -\Pi_i^{SE}(t)\rho_i^S(t)\,, \tag{1}$$

$$\dot{\rho}_i^E = -\eta\rho_i^E(t) + \Pi_i^{SE}(t)\rho_i^S(t)\,, \tag{2}$$

$$\dot{\rho}_i^P = \left[-\alpha - \Pi_i^{CT}(t) - \Pi_i^{VD}(t)\right]\rho_i^P(t) + \eta\rho_i^E(t)\,, \tag{3}$$

$$\dot{\rho}_i^{I_A} = \left[-\mu - \Pi_i^{CT}(t) - \Pi_i^{VD}(t)\right]\rho_i^{I_A}(t) + (1-p)\alpha\rho_i^P(t)\,, \tag{4}$$

$$\dot{\rho}_i^{I_S} = \left[-\mu - \delta - \Pi_i^{CT}(t) - \Pi_i^{VD}(t)\right]\rho_i^{I_S}(t) + p\alpha\rho_i^P(t)\,, \tag{5}$$

$$\dot{\rho}_i^D = -\gamma\rho_i^D(t) + \delta\rho_i^{I_S}(t) + \left[\Pi_i^{CT}(t) + \Pi_i^{VD}(t)\right]\left[\rho_i^P(t) + \rho_i^{I_A}(t) + \rho_i^{I_S}(t)\right] \tag{6}$$

$$\dot{\rho}_i^R = \gamma\rho_i^D(t) + \mu\left[\rho_i^{I_A}(t) + \rho_i^{I_S}(t)\right]\,, \tag{7}$$

Since the sum of probabilities associated to a node i must remain equal to 1 we have:

$$\dot{\rho}_i^S(t) + \dot{\rho}_i^E(t) + \dot{\rho}_i^P(t) + \dot{\rho}_i^{I_A}(t) + \dot{\rho}_i^{I_S}(t) + \dot{\rho}_i^D(t) + \dot{\rho}_i^R(t) = 0, \tag{8}$$

so that the set of 7 equations per node can be reduced to 6, yielding a set of $6N$ coupled differential equations for the whole system.

Now let us describe the terms associated to transitions due to pairwise or group interactions. In the former set of equations, these transitions are captured by the rates Π_i^{SE}, Π_i^{CT} and $\Pi_i^{VD}(t)$ that account for Infections, Contact Tracing Detections and Virtual Detections respectively. These three rates read as follows:

$$\Pi_i^{SE}(t) = \sum_{j=1}^{N} a_{ij}\left\{\beta_A\left[\rho_j^P(t) + \rho_j^{I_A}(t)\right] + \beta_S\rho_j^{I_S}(t)\right\}\,, \tag{9}$$

$$\Pi_i^{CT}(t) = \sum_{j=1}^{N} a_{ij} f^2 \rho_j^D(t)\,, \tag{10}$$

$$\Pi_i^{VD}(t) = \sum_{m=1}^{M}\sum_{\alpha=1}^{\kappa_i^{(m)}} \Xi_i(\sigma_\alpha^{i\,(m)})\,. \tag{11}$$

As anticipated, Eqs. (9) and (10), accounting for the Infection and Contact Tracing detection rates, are built upon summing over the contributions from physical neighbors of node i, i.e. mediated by the elements of the ith row of the adjacency matrix $\mathbf{A}$. In contrast, the last expression, Eq. (11), accounts for the detection rate due to the dissemination of SRDAs through hyperedges and, therefore, the rate comprises the sum across all possible orders and, for each order m, it considers each of the $\kappa_i^{(m)}$ groups in the set $\mathcal{E}_i^{(m)}$.

The modeling of the contribution of each group to the detection rate, denoted in Eq. (11) as $\Xi_i(\sigma_\alpha^{i\,(m)})$, reads as follows:

$$\Xi_i(\sigma_\alpha^{i\,(m)}) = \xi^{(m)} D(\sigma_\alpha^{i\,(m)})\left[\frac{\sum_{j\in\sigma_\alpha^{i\,(m)}}\rho_j^D(t)}{m}\right]^{\nu^{(m)}}\,, \tag{12}$$

where $D(\sigma_\alpha^{i\,(m)})$ is the expected number of detected neighbors of node i belonging to the virtual hyperedge of order m $\sigma_\alpha^{i\,(m)}$ with which node i also has physical interaction. This quantity reads:

$$D(\sigma_\alpha^{i\,(m)}) = \sum_{j\in\sigma_\alpha^{i\,(m)}}\left[\Delta_{ij}^{(m)}\rho_j^D(t)\right]. \tag{13}$$

The expression in Eq. (12) can be explained as follows: $\xi^{(m)}$ is the rate at which the result is obtained once the node i decides to go testing, this rate is activated (and multiplied) by the number of SRDAs launched in the group which are also physical contacts of i, Eq. (13), while the last term accounts for an echo chamber effect that captures the synergy with the group towards testing. Therefore, synergy results from a peer pressure created by the group chat environment and becomes more relevant when the relative fraction of positives present in the group is large. This last term is also modulated by an exponent $\nu^{(m)}$ which controls the non-linearity of the synergistic detection process. This way, in a similar way as introduced in [46,47], social reinforcement (inhibition) to undergo testing corresponds to rates $\nu^{(m)} < 0$ ($\nu^{(m)} > 0$). The linear contribution, i.e. $\Xi_i(\sigma_\alpha^{i\,(m)}) = \xi^{(m)} D(\sigma_\alpha^{i\,(m)})$, is recovered by setting $\nu^{(m)} = 0$.

Finally, let us note that the expression chosen $\Pi_i^{VD}(t)$ is inspired by the infection rate introduced by St-Onge et al. [48] in the context of social spreading dynamics. In this latter case, the infection rate for a healthy node through one of its hyperedges increases with the number of infectious neighbors within that hyperedge, in contrast to traditional approaches on simplicial models of social contagion [28], in which the infection pathway through a particular hyperedge is only activated in case all the acquaintances belonging to this hyperedge are infectious.

3. The dynamics of *Self-Reported Digital Alerts*

In this section we analyze the dynamics of contagion processes in competition with the spread of detection cascades by exploring the dynamical behavior of the $SEPI_AI_SR$ model introduced above. Our analysis are carried out by integrating the set of Eqs. (1)–(7) from a initial condition consisting on a small infectious seed homogeneously distributed ($\rho_i^E(0) = 0.01,\ \forall i \in N$). The dynamics is then analyzed until the unique equilibrium in which the population splits between susceptible and recovered (i.e. $\rho_i^S + \rho_i^R = 1,\ \forall i \in N$) is reached. This analysis enables us to unveil and characterize the contribution of the dissemination of SRDAs to the mitigation of epidemic waves in the following sections.

3.1. Self-Reported Digital Alerts versus Contact tracing

We start analyzing the individual effect of Virtual Detections on epidemic control by assuming, as a first approach, that both physical and virtual interactions take place on the same pairwise network (so that group interactions do not apply at this stage and $M = 1$) and that synergy is linear $\nu^{(1)} = 0$.

In Fig. 2(a) we show the time evolution of the fraction of individuals that are infected at time t,

$$c(t) = \frac{1}{N}\sum_{i=1}^{N}\rho_i^S(t)\Pi_i^{SE}(t), \tag{14}$$

using as the backbone for physical and virtual interactions the face-to-face contact data from an American high school [44], whose characteristics are summarized in Table 2. Considering, as anticipated above, a negligible fraction of symptomatic detection $\delta = 0.05$ to trigger detection and removing the contribution of Contact Tracing by setting $f = 0$, we observe how the dissemination of SDRAs behind VD promotes the bending of the epidemic curve, i.e. the anticipation and reduction of the epidemic peak. In particular, larger values of $\xi = \xi^{(1)}$ lead to a faster (and larger) mitigation, providing an alternative way to bend the epidemic curve without the need to implement CT applications in mobile phones.

To illustrate the isolated and intertwined effect of detection strategies (CT and VD), we show in Fig. 2(b) the attack rate,

$$r^\infty = \lim_{t\to\infty}\frac{1}{N}\sum_{i=1}^{N}\rho_i^R(t), \tag{15}$$

with respect to both ξ and f. The shape of the contour lines indicates the complementary effect of the two detection strategies. Nevertheless, VD reduces the epidemic size more than CT, e.g., while the curve of $r^\infty = 0.7$ crosses the x-axis (absence of VD) at $f \approx 0.7$, it only requires $\xi \approx 0.5$ to achieve the same attack rate in the absence of CT (when the curve crosses the y-axis). The reason behind this asymmetry between CT and CD has its roots on the functional form of the VD rate, Eq. (11).

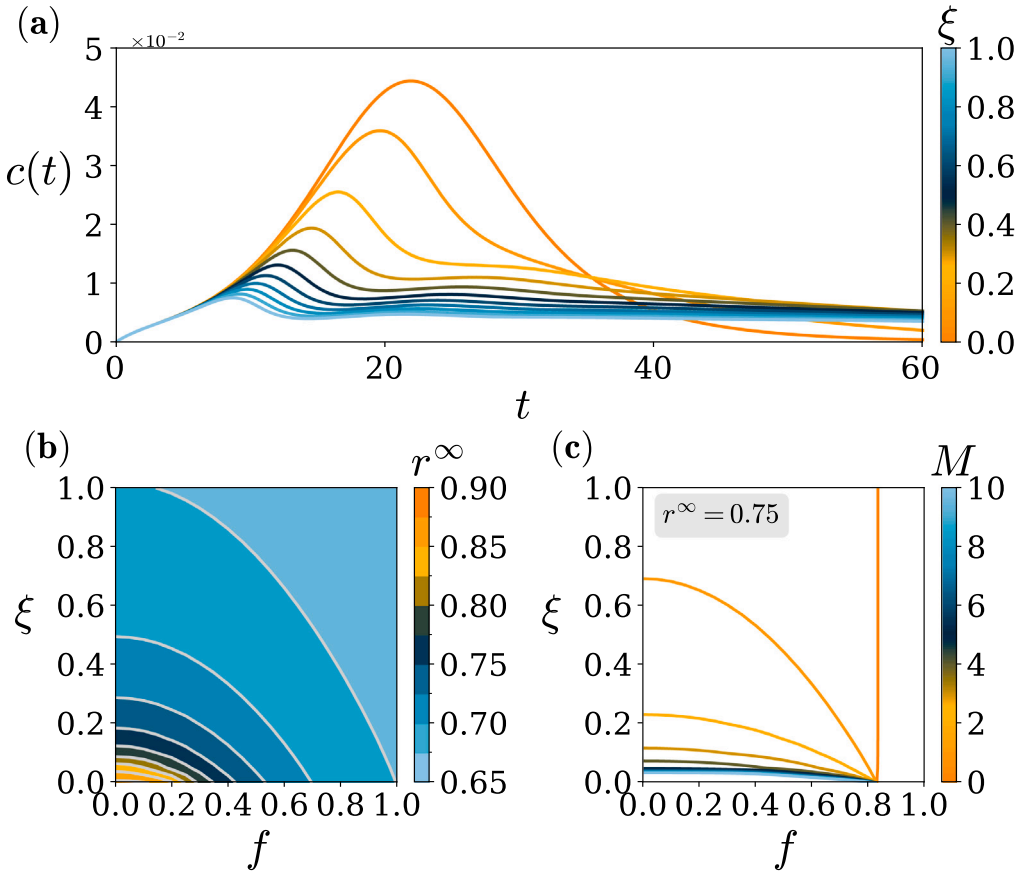

Fig. 2. Virtual Detection bends the epidemic wave. (a) Temporal evolution of the fraction of new contagions given $\delta = 0.05$ and $f = 0$. Both physical and virtual interactions are represented by a school proximity network. Each line represents a different value of ξ. (b) Joint outcome in the attack rate r^∞ between the influence of Digital Contact Tracing and SRDA strength. Both physical and virtual interactions are represented by a school proximity network, and $\delta = 0.05$. (c) Map between the minimum strength of CT and VD needed to reach $r^\infty = 0.75$, for different maximum interaction orders. The physical and virtual interactions are represented by a synthetic random hypergraph with maximum downward closure, and $\delta = 0.05$.

In particular, when restricting (as it is the case in Fig. 2(b)) to pairwise and linear interactions the former rate reads:

$$\Pi_i^{VD}(t) = \sum_{j=1}^{N} \left[a_{ij} \xi \rho_j^D(t) \right] , \tag{16}$$

showing a linear dependency on ξ. In contrast, the rate associated to CT, Eq. (10), depends quadratically on f, so that, in order to have similar detection rates for both mechanisms, we need $\xi \sim f^2$.

Furthermore, Fig. 2(b) shows that the effectiveness of both CT and VD in reducing the epidemic attack rate saturates for intermediate and large values of ξ and f. Recall that both strategies rely on the propagation of detection cascades that operate through the interaction of infectious and detected individuals. Thus, since both CT and DV are activated after the first (symptomatic) detections, both are very effective when there are many infected individuals. However, in a situation of low incidence, such as during the decay of the epidemic wave (see Fig. 2(a)), this efficacy drops considerably and, as a result, many individuals end up being infected in the last phase of the epidemic, thus increasing the final attack rate. These findings underscore the importance of the combined effect of symptomatic detection and interaction-based detection, which is optimal for reducing the attack rate of an epidemic virus, as demonstrated in [5].

3.2. Influence of higher-order interactions

So far, we have studied how VD policy effectively bends the epidemic curve by hindering the spread of a pathogen. In this subsection, we extend our analysis to scenarios where the SRDAs spread through groups of different sizes. To study the effect of virtual hyperedges of different order in the range $m \in [1, M]$, we make use of a synthetic random hypergraph whose nodes have in average the same number of hyperedges, i.e. generalized degree, across all types and orders of interactions, and in which all the hyperedges of order m are faces of the hyperedges of order $m + 1$ (the details about the crafting are in Appendix A). In particular, we set $\langle k \rangle = \langle \kappa^{(m)} \rangle = 12, \ \forall m \in [1, M]$ and $N = 500$.

In Fig. 2(c) we plot the combinations of parameters f-ξ needed to reduce the epidemic size from the baseline value $r^\infty = 0.9$ to $r^\infty = 0.75$ for different values of M (the maximum order of hyperedges present in the hypergraphs). Obviously, in the absence of virtual interactions, $M = 0$, we observe that the function in the (f, ξ)-plane does not depend on ξ and a value $f \approx 0.8$ is required to reach $r^\infty = 0.75$. For $M = 1$, i.e. both detection pathways occur through pairwise interactions, and hence we recover the a function with a equivalent shape to what was shown in Fig. 2(b). For $M > 1$, as more orders of interactions are taken into account, the shape of the function become more asymmetric since the cumulative nature of higher-order interactions promotes detection beyond what is achievable by pairwise physical interactions alone. This enhancement of mitigation resembles similar boosting phenomenology reported in other dynamical processes with higher-order interactions at work [18,27,28], such as the increment of prevalence in the active phase of social contagion dynamics [28] or the enlargement of the stability region of ensembles of coupled oscillators [27].

Finally, let us note that the detection boost provided by groups can be facilitated or hindered depending on the synergy exponent. In particular, if $\nu^{(m)} < 0$ the alarm perception of individuals is amplified and

epidemic control is strengthened. Conversely, if group conversations lead to an underestimation of risk ($\nu^{(m)} > 0$), then the effectiveness of the policy is downgraded. Further details can be found in Appendix B.

4. Virtual Detection in real networks

We now turn our attention to more realistic scenarios. In addition to the real networks (reported in Table 2) constituting the backbone of physical interactions, for the virtual hypergraph we now build synthetic collections of groups based on statistics about Whatsapp private communities. To create these virtual hypergraphs, we analyze the extensive dataset collected by Seufert et al. [49], which consists of 5956 private WhatsApp chat histories containing over $76 \cdot 10^6$ messages from more than 117000 users.

4.1. Crafting virtual hypergraphs from real data

The anonymization process of the aforementioned Whatsapp data performed by the authors of [49] impedes to reconstruct the actual virtual communication hypergraph. Nevertheless, we have extracted the main features to create a synthetic set of virtual groups. Specifically, we build our synthetic data on three facts inferred from the distribution of groups (more details in Appendix C). Namely: (*i*) chats of 2-members chats represent the 39% of virtual interactions, (*ii*) the size distribution of groups with more than 2 members follows a long-tailed function, and (*iii*) groups with over 50 members represent less than the 10% of the chats.

With the former three ingredients we construct the backbone of virtual interactions that completes, together with the network of physical contacts, the interaction map of a system. In fact, since both the network of contacts and the virtual hypergraph share the same set of individuals and considering that these tend to have virtual connections with those people with whom they interact physically, we consider as potential virtual interactions all the cliques that appear in the physical networks, i.e. $\Delta_{ij}^{(m)} = 1, \ \forall i,j,m$. Obviously, since these cliques from the physical network do not obey the statistical laws observed in real data about interaction groups we must sample out the final virtual interactions out of them. The rules to decide which cliques remain are as follows. First, the virtual interactions of order 1 (links) are chosen to be coincident with the physical pairwise network. Note that those physical edges chosen to be also virtual ones will represent the 39% of the total number of hyperedges. Afterwards, we sample the remaining 61% of the virtual interactions of order $m > 1$ from the cliques of size $m+1$ in the physical network. We make the selection of the cliques of each order by following the distribution of number of groups, originally inferred for $m \in [3, 50]$ on the Whatsapp dataset [50].

The hypergraphs constructed as explained above yield structures with maximal correlation between physical and virtual interactions, i.e. all virtual interactions are also present in the physical contact network. However, people do not interact physically with all the people they interact with virtually. Thus, to construct hypergraphs in which the correlation between physical and virtual interactions can be tuned we define a metric that quantifies the fraction of pairwise projections of virtual interactions of order m that exist as edges in the network of physical contacts:

$$\Theta^{(m)} = \frac{\sum_{i=1}^{N}\sum_{j=1}^{N}\Delta_{ij}^{(m)}}{\sum_{i=1}^{N}\sum_{j=1}^{N}\hat{a}_{ij}^{(m)}}. \tag{17}$$

Equipped with this metric we take the hypergraphs that were originally constructed out of the physical cliques, i.e. with maximal correlation $\Theta^{(m)} = 1, \ \forall m \in [1, M]$, and proceed to make a sequential rewiring of the set of hyperedges of order m, accepting changes when they minimize $\Theta^{(m)}$. This way, we can tune $\Theta^{(m)}$ to cover the whole range of values $\Theta^{(m)} \in [0, 1]$, achieving a one-parameter family of hypergraphs that allows to study the influence of the correlation between groups of order m and physical edges in the dynamics of VD. In the following, we will consider that the former correlation does not depend of the size of groups so that $\Theta = \Theta^{(m)} \ \forall m \in [1, M]$.

4.2. Virtual Detection fosters epidemic control

Once constructed the virtual hypergraphs based on both the physical contact networks and the statistical properties of online groups, we can finally assess the effect of VD based on SRDAs dissemination in close-to-reality scenarios. Considering that average number of messages is independent of the group size [49] and that this size does not influence the time spanned between receiving the SRDAs and testing, we set $\xi^{(m)} = \xi, \ \forall m$ (more details in Appendix C). In addition, for the sake of simplicity, we do not consider group synergy, i.e. $\nu^{(m)} = 0$. Therefore, we use as control parameters the rate of testing after receiving SRDAs (ξ), and the correlation between physical and virtual interactions (Θ).

In Fig. 3 we show the evolution of the fraction of newly infected agents over time for each of the physical contact networks reported in Table 2. The epidemic curve in the absence of detection ($\delta = 0$) is shown to compare with the other scenarios in which different detection pathways operate. In particular, we consider the case when SD ($\delta = 0.5$) and CT are at work, being the latter characterized by a penetration of $f = 0.21$, i.e. the adoption rate of the application *Radar Covid* in Spain [16]. In all the cases, the combination of SD and CT does not achieve bending the epidemic curve but flattens it. While detection policies reduce the peak of the new contagions curve, the area within the curve is still of a considerable magnitude. Next, the case when VD is implemented ($\xi = 0.5$, $\Theta = 0.5$) alone (triggered by a negligible fraction of SD ($\delta = 0.05$)) shows a qualitatively different scenario. In almost all the cases VD is able to bend the epidemic curve thus anticipating and achieving a significant reduction of the peak. Finally, the fraction of new contagions in the case all the available detection policies are implemented ($\delta = 0.5$, $f = 0.21$, $\xi = 0.5$ and $\Theta = 0.5$) shows the largest degree of mitigation. However, these results do not improve much with respect to VD alone, indicating the power of the latter to alter the epidemic trajectory.

As anticipated above, the effect of VD varies across the different networks considered. In particular, although in most cases VD provokes a clear bending of the epidemic curve, in panels (c)–(f), a second peak shows up after the first one is bent, thus leading to a scenario compatible with a flattened epidemic. In all cases, the reduction on the peak is accompanied by an increment on the effective duration of the epidemic wave. In particular, the dense topologies in panels (g)–(h) give rise to an almost negligible peak at the expense of an extremely long relaxation time, more akin to an endemic equilibrium than to a decaying epidemic wave advancing toward the final absorbing state.

To round off, we analyze the role of the correlation between virtual and physical interactions. Fig. 4 shows the attack rate, r^{∞}, as a function of the correlation, Θ, for all the network structures in Table 2. When VD is the unique detection pathway at work, Fig. 4(a), the correlation between virtual and physical networks yield a smaller attack rate as shown by the monotonically decreasing dependence and a tendency to a plateau as $\Theta \to 1$. This plateau is a consequence of how bending strategies excel at anticipating and suppressing the epidemic peak at the expense of increasing the relaxation time until the absorbent state. This extremely long relaxation thus provoke that the reduction of the attack rate is not significantly altered with Θ. In fact, in this regime, r^{∞} can be significantly reduced when symptom detection is increased as shown in panel Fig. 4(b) for which $\delta = 0.5$. Moreover, regardless of the symptomatic detection rate, the effectiveness of detection policies is minimal when $\Theta \to 0$, for which the reduction in the attack rate is found to depend solely on the symptomatic detection and contact tracing rates. Notably, low values of structural correlations are expected in random hypergraphs in the thermodynamic limit ($N \to \infty$). Therefore, in the event of the virtual interactions being crafted at random, the effectiveness of virtual detection would be negligible.

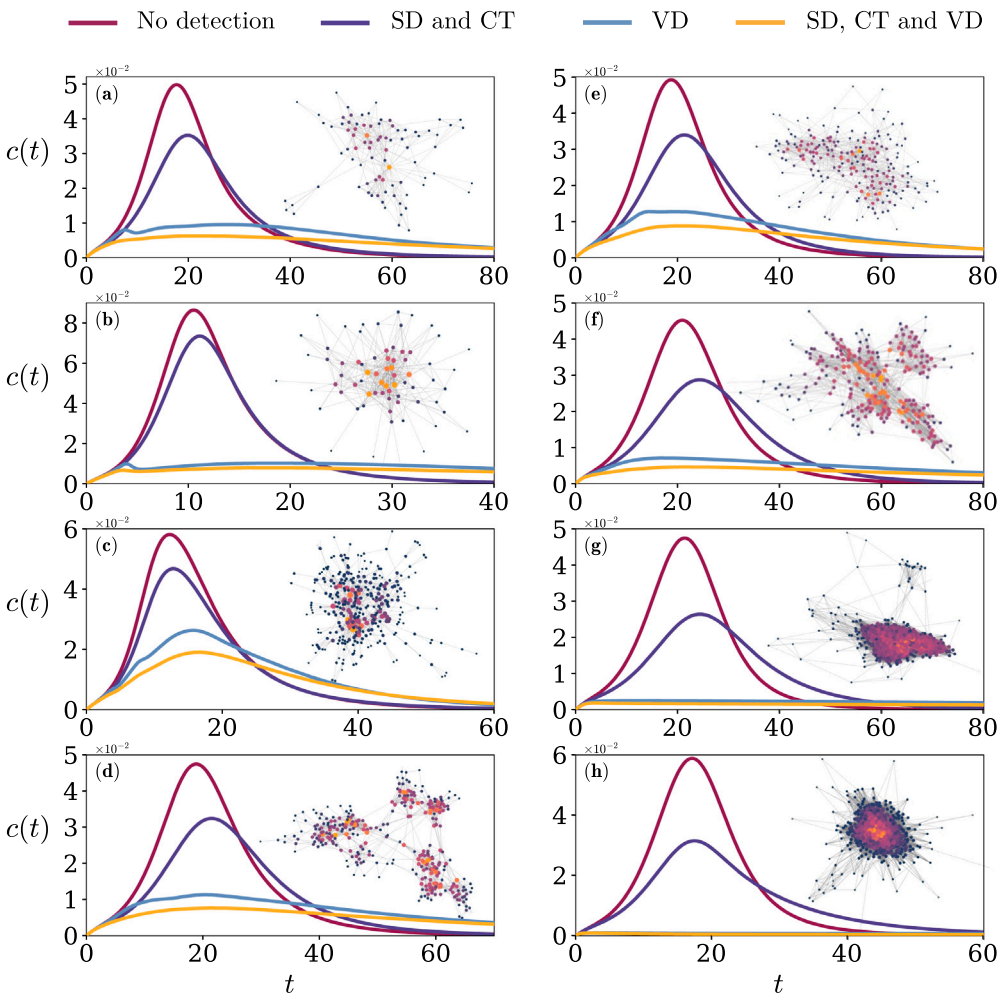

Fig. 3. Epidemic control in real datasets. Evolution of the fraction of new contagions when different detection policies are implemented, in different social context. Each panel (a)–(h) is accompanied by the graphical representation of the real dataset: (a) Malaui village, (b) hospital, (c) scientific conference, (d) French high school, (e) workplace, (f) primary school, (g) American high school and (h) university. In all panels the wine curve depicts the epidemic wave in absence of detection measures ($\delta = 0$). The purple curve shows the result of the combination of SD ($\delta = 0.5$) and CT ($f = 0.21$). The blue curve represents the influence of Virtual Detection ($\xi = 0.5$, $\Theta = 0.5$) triggered by a negligible fraction of SD ($\delta = 0.05$). Finally, the yellow curve is the fraction of new contagions in case all detection policies are implemented ($\delta = 0.5$, $f = 0.21$, $\xi = 0.5$ and $\Theta = 0.5$). (For interpretation of the references to color in this figure legend, the reader is referred to the web version of this article.)

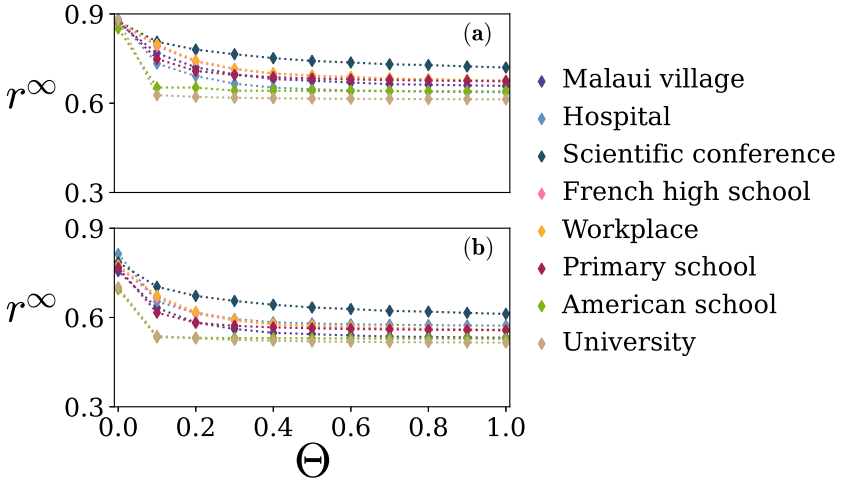

Fig. 4. Correlation between physical and virtual interactions drives the effectiveness of Virtual Detection. Attack rate, r^∞, as a function of the degree of correlation, Θ, for (a) $\delta = 0.05$, $f = 0$ and $\xi = 0.5$ and (b) $\delta = 0.5$, $f = 0.21$ and $\xi = 0.5$. Each data series corresponds to a real dataset as indicated in the legend.

5. Conclusions

Control policies have proven to be key in containing an epidemic outbreak. Together, pharmaceutical measures (e.g. vaccines [51]), preventive measures (e.g non-pharmaceutical interventions such as social distancing [52], prophylactic measures [36] and awareness campaigns [53,54]), and reactive measures (e.g. Contact Tracing [5,6]), all have a complementary effect in reducing the effective number of future infections. In particular, reactive measures can reduce the infectious period by detecting the infectious population early. However, Digital Contact Tracing requires the population to download mobile applications which, unfortunately, have shown low adoption rates [16]. Conversely, individual awareness driven by the dissemination of *Self-Reported Digital Alerts* (SRDAs) through the communication groups inherent in today's virtual society could serve to overcome these adoption barriers.

In this work we have illustrated how the dissemination of SRDAs provides a virtual detection pathway able at bending the epidemic curve, thus lowering and advancing its peak. Moreover, we have analyzed it as a group-based interaction between individuals in which the additive nature and synergy characteristics of higher-order interactions play an important role in fostering detection. Our approach includes higher-order interactions in detection scenarios in a different way than percolation-based approaches used in Digital Contact Tracing [55], that consider blocking infection pathways in case the potentially infectious individuals have a digital application. Instead, here higher-order interactions are incorporated as an intrinsic characteristic of today's society, showing how this feature can enhance epidemic control organically.

After a careful study about how virtual detection depends on different ingredients of the interaction backbone, we have found that this policy achieves its best performance when the overlap between physical and virtual connections is large. Therefore, it is most effective in controlled environments with recurrent contacts, with whom people are more likely to also have virtual interactions. Our results could be inspiring for prevention campaigns. In particular, it would be beneficial for such campaigns to consider promoting the establishment of straightforward virtual communication between individuals who are engaged in a coincident activity that necessitates physical interaction. This could be achieved by creating "*virtual bubbles*", which would facilitate communication between individuals attending to the activity, regardless of whether it is recurrent, such as attending a regular lecture, or just a single event. In the latter situation, the virtual communication structure would notably expand, encompassing numerous physical interactions that would otherwise result in undetectable contagions. In any case, to better reflect reality, further efforts should be made to obtain closed datasets that take all communication methods into account. In this direction, Sapiezynski et al. [45] described a multi-layer temporal network that includes the proximity network among participants, as well as the network of SMS messages, phone calls, and Facebook friendships. Nevertheless, as online message applications have overtaken traditional communication methods [56], it is necessary to consider online chats to better assess this issue with real data.

The conclusions drawn by our study and the higher-order framework presented should be further enriched in the future with more ingredients and data from encrypted applications like Whatsapp. The inclusion of real data would provide insights into the microscopical organization of higher-order structures, which has been shown to have a significant impact on collective phenomena [32,57–59]. However, this research avenue is challenging since, on the one hand, studies on private groups use anonymized data, thus making it impossible to track the same individual across different groups [49,60,61], and, on the other hand, available studies on public groups are not representative of the typical use of Whatsapp [62].

Another potential direction for future research could be the refinement of the model to encompass the role of asymmetry in virtual interactions, along with other subtle aspects of virtual interactions. Moreover, as previously stated when introducing the model, the efficacy of reactive control strategies, such as contact tracing and virtual detection, depends on the actions of the detected individuals, who are expected to self-isolate and therefore stop spreading the disease. In order to incorporate the impact of defectors into the model, the detection rates could be refined in a manner analogous to that described in Ref. [63], where the detection rates depend on the availability of resources. This refinement would yield the conclusion that an increase in the number of defectors results in a corresponding decrease in the efficiency of detection policies. Other future research avenues include exploring virtual detection under limited resources [63], analyzing detection processes in contexts where multiple concomitant strains are involved [47,64,65], and investigating the influence of temporal resolution on detection processes, given recent advances in understanding temporal higher-order interactions [66,67].

CRediT authorship contribution statement

Santiago Lamata-Otín: Writing – original draft, Investigation, Formal analysis, Data curation, Conceptualization. **Adriana Reyna-Lara:** Writing – original draft, Investigation, Data curation, Conceptualization. **Jesús Gómez-Gardeñes:** Writing – original draft, Investigation, Formal analysis, Conceptualization.

Declaration of competing interest

The authors declare that they have no known competing financial interests or personal relationships that could have appeared to influence the work reported in this paper.

Data availability

The SocioPatterns datasets were downloaded from https://www.sociopatterns.org/datasets and the Copenhagen dataset was downloaded from https://doi.org/10.6084/m9.figshare.7267433. The WhatsApp data was downloaded from https://figshare.com/articles/dataset/WhatsApp_Data_Set/19785193.

Acknowledgments

S.L.O and J.G.G. acknowledge financial support from the Departamento de Industria e Innovación del Gobierno de Aragón y Fondo Social Europeo, Spain (FENOL group grant E36-23R) and from Ministerio de Ciencia e Innovación, Spain (grant PID2020-113582GB-I00). S.L.O. acknowledges financial support from Gobierno de Aragón, Spain through a doctoral fellowship.

Code availability statement

The code is available at: https://github.com/santiagolaot/higher-order-epidemic-control.

Appendix A. Hypergraphs with maximum downward closure

To build a random hypergraph with maximum downward closure and average generalized degrees $\langle \kappa^{(m)} \rangle = z, \ \forall m \in [1, M]$, we start form a set of randomly chosen hyperedges of order M with $\langle \kappa^{(M)} \rangle = z$. Then, among all the subsets of order $m = M-1$ within the connections, we randomly select as many as necessary to have the desired average generalized degree $\langle \kappa^{(m)} \rangle = z$. We repeat this procedure iteratively until we obtain a pairwise backbone with $\langle \kappa^{(1)} \rangle = z$. Following the naive assumption that the pairwise virtual interactions and the physical interactions are coincident, we have our synthetic structure with $\langle k^{(1)} \rangle = z$ and $\langle \kappa^{(m)} \rangle = z, \ \forall m \in [1, M]$.

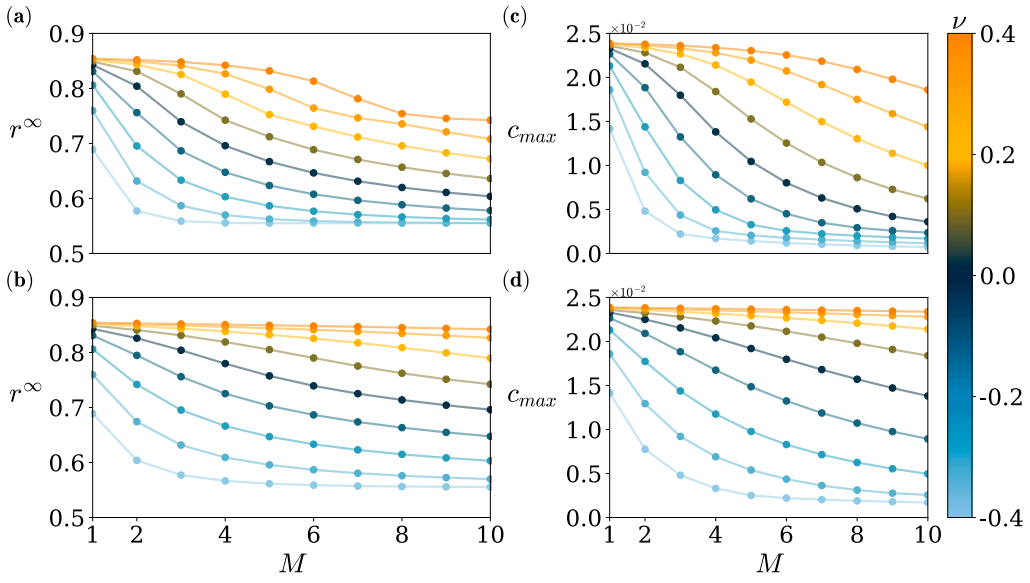

Fig. B.5. Group synergy in Virtual Detection drives epidemic control. (a)–(b): Impact of the non-linearity of group detection on the attack rate. Panel (a) shows the cumulative impact up to order M and panel (b) shows the individual for each order. (c)–(d): Impact of the non-linearity of group detection on the peak of the epidemic. Panel (c) shows the cumulative impact up to order M and panel (d) shows the individual for each order. In all panels $k = 12$, $\kappa^{(m)} = 6$, $\xi^{(m)} = 0.5$ and $\Theta^{(m)} = 0.5\ \forall m$.

Appendix B. Influence of group synergy on Virtual Detection

In this appendix, we analyze how Virtual Detection performance depends on the group synergy. To facilitate a better understanding, we assume a mean field hypothesis, i.e. that all individuals in the network are equivalent. We only maintain the heterogeneity in the distribution of the number of virtual interactions per orders, by considering that nodes have $\kappa^{(m)}$ interactions per order. We impose that $\rho_i^Y = \rho^Y,\ \forall i \in N$ and $Y \in [S, E, P, I_A, I_S, D, R]$, and therefore, the set of Eqs. (1)–(7) now accounts for the evolution of fraction of population on each of the states.

The transition probabilities ($\Pi_i^{SE}(t) = \Pi_i^{SE}(t)$, $\Pi_i^{CT}(t) = \Pi^{CT}(t)$ and $\Pi_i^{VD}(t) = \Pi^{VD}(t)$) depending on the physical and virtual interactions read:

$$\Pi^{SE}(t) = k\left\{\beta_A\left[\rho^P(t) + \rho^{I_A}(t)\right] + \beta_S\rho^{I_S}(t)\right\}, \tag{B.1}$$

$$\Pi^{CT}(t) = kf^2\rho^D(t). \tag{B.2}$$

$$\Pi^{VD}(t) = \sum_{m=1}^{M}\left\{\kappa^{(m)}\xi^{(m)}D^{(m)}\left[\rho^D(t)\right]^{\nu^{(m)}}\right\}. \tag{B.3}$$

The expected number of detected neighbors belonging to a virtual hyperedge of order m with which a node also has physical interaction is:

$$D^{(m)} = m\Theta^{(m)}\rho^D(t), \tag{B.4}$$

where $\Theta^{(m)}$ is the average correlation between physical interactions and virtual interactions of order m.

In Fig. B.5(a)–(b), we show how Virtual Detection performance depends on the synergistic nature of virtual interactions. For simplicity purposes, we assume that the non-linearity of the synergistic detection is the same along all orders, i.e. $\nu^{(m)} = \nu,\ \forall m \in [1, M]$. Panel (a) shows the effect of virtual interactions up to order M on reducing the final size of the epidemic, and panel (b) separates the contribution of each order M. In the presence of social reinforcement ($\nu < 0$), Virtual Detection has an effectiveness beyond what is achievable in the linear situation. In contrast, in the case of social inhibition ($\nu > 0$), the attack rate values get closer to their original value as the non-linearity increases.

Moreover, in B.5(c)–(d) we complement our analysis showing the value of the peak of new contagions, defined as:

$$c_{\max} = c(t)|_{\max} = \Pi^{SE}(t)\rho^S(t)|_{\max}. \tag{B.5}$$

The observed tendency is analogous to that observed for the attack rate. However, it is notable that while the peak becomes negligible in the context of strong social reinforcement situations, in the stationary state of the dynamics more than 50% of the population end up in the recovery compartment, indicating that they have been infected in the last phase of the epidemic. This finding is consistent with the results presented in Fig. 2(b) of the main text.

It is important to note that the mean-field description (and, in particular, Eqs. (B.3), (B.4)) also facilitates the understanding of the effect of the virtual generalized degree $\kappa^{(m)}$, the rate of Virtual Detection $\xi^{(m)}$, the group size m and the correlation between physical and virtual interactions $\Theta^{(m)}$. Notably, their roles in the formula are interchangeable in the linear case, i.e. $\nu = 0$, with large values of the parameters fostering Virtual Detection. Furthermore, it is notable that, in the event that we posit that large groups are associated with low values of correlation between physical and virtual interactions, there would be a trade-off between the group size, m, and the correlation, $\Theta^{(m)}$. Consequently, an optimal group size for optimizing Virtual Detection could be identified.

Appendix C. Insights obtained from Whatsapp data

In this appendix we extract insights from the dataset collected by Seufert et al. [49], which consists of 5956 private WhatsApp chat histories containing over 76 million messages from more than 117,000 users. In Fig. C.6(a) we show the distribution of active users per chat in log–log scale. There is a clear shift from the number of chats with 2 people to the number of chats with more than 2 people. In particular, the cumulative distribution shows how chats with 2 people represent the 39% of the total number of chats. For chats with more than 2 members the distribution follows a long-tailed functional form. Furthermore, chats with more than 50 active members represent the 10% of the total number of chats and thus there is a clear lack of statistics, which is noticeable by the dispersion on the average number of messages per chat size shown in Fig. C.6(b). This average number of messages per chat size seems to be almost independent of the chat size.

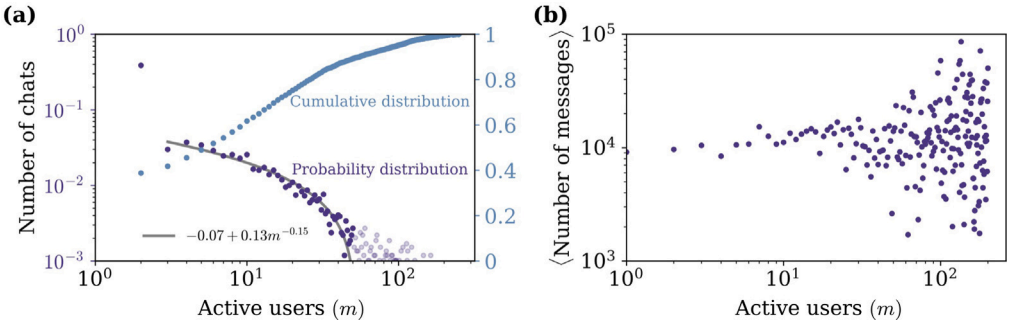

Fig. C.6. Insights obtained from the dataset collected by Seufert et al. [49]. (a) Distribution of the number of chats in terms of the number of active users per chat. (b) Average number of messages in terms of the number of active users per chat.

References

[1] Tilahun B, Gashu KD, Mekonnen ZA, Endehabtu BF, Angaw DA. Mapping the role of digital health technologies in prevention and control of covid-19 pandemic: review of the literature. Yearb Med Inform 2021;30:026–37.

[2] Fagherazzi G, Goetzinger C, Rashid MA, Aguayo GA, Huiart L. Digital health strategies to fight covid-19 worldwide: challenges, recommendations, and a call for papers. J Med Internet Res 2020;22:e19284.

[3] Centers for Disease Control and Prevention. Webpage. 2024, https://www.cdc.gov/coronavirus/2019-nCoV/index.html. [Accessed 14 February 2024].

[4] Group CPH, Anglemyer A, Moore TH, Parker L, Chambers T, Grady A, et al. Digital contact tracing technologies in epidemics: A rapid review. Cochrane Database Syst Rev 2020.

[5] Reyna-Lara A, Soriano-Paños D, Gómez S, Granell C, Matamalas JT, Steinegger B, et al. Virus spread versus contact tracing: Two competing contagion processes. Phys Rev Res 2021;3:013163.

[6] Kojaku S, Hébert-Dufresne L, Mones E, Lehmann S, Ahn Y-Y. The effectiveness of backward contact tracing in networks. Nature Phys 2021;17:652–8.

[7] Barrat A, Cattuto C, Kivelä M, Lehmann S, Saramäki J. Effect of manual and digital contact tracing on covid-19 outbreaks: A study on empirical contact data. J R Soc Interface 2021;18:20201000.

[8] Keeling MJ, Hollingsworth TD, Read JM. Efficacy of contact tracing for the containment of the 2019 novel coronavirus (covid-19). J Epidemiol Community Health 2020.

[9] Bianconi G, Sun H, Rapisardi G, Arenas A. Message-passing approach to epidemic tracing and mitigation with apps. Phys Rev Res 2021;3:L012014.

[10] Burgio G, Steinegger B, Rapisardi G, Arenas A. Homophily in the adoption of digital proximity tracing apps shapes the evolution of epidemics. Phys Rev Res 2021;3:033128.

[11] Bassolas A, Santoro A, Sousa S, Rognone S, Nicosia V. Optimizing the mitigation of epidemic spreading through targeted adoption of contact tracing apps. Phys Rev Res 2022;4:023092.

[12] Nielsen BF, Sneppen K, Simonsen L, Mathiesen J. Differences in social activity increase efficiency of contact tracing. Eur Phys J B 2021;94:1–11.

[13] de Meijere G, Castellano C. Limited efficacy of forward contact tracing in epidemics. Phys Rev E 2023;108:054305.

[14] Burdinski A, Brockmann D, Maier BF. Understanding the impact of digital contact tracing during the covid-19 pandemic. PLOS Digital Health 2022;1:e0000149.

[15] Burdinski A, Brockmann D, Maier BF. Digital contact tracing contributes little to covid-19 outbreak containment. 2021, medRxiv 2021–06.

[16] Penentration rate of 'radar covid' (Spain). 2022, Webpage, https://radarcovid.gob.es/estadisticas/descargas-radar. [Accessed 25 September 2022].

[17] Whatsapp usage. 2024, Webpage, https://www.statista.com/markets/424/topic/538/mobile-internet-apps/#overview. [Accessed 6 February 2024].

[18] Battiston F, Cencetti G, Iacopini I, Latora V, Lucas M, Patania A, et al. Networks beyond pairwise interactions: Structure and dynamics. Phys Rep 2020;874:1–92.

[19] Majhi S, Perc M, Ghosh D. Dynamics on higher-order networks: A review. J R Soc Interface 2022;19:20220043.

[20] Bick C, Gross E, Harrington HA, Schaub MT. What are higher-order networks? SIAM Rev 2023;65:686–731.

[21] Di Gaetano L, Battiston F, Starnini M. Percolation and topological properties of temporal higher-order networks. Phys Rev Lett 2024;132:037401.

[22] Sun H, Bianconi G. Higher-order percolation processes on multiplex hypergraphs. Phys Rev E 2021;104:034306.

[23] Bianconi G, Dorogovtsev SN. Theory of percolation on hypergraphs. Phys Rev E 2024;109:014306.

[24] Tanaka T, Aoyagi T. Multistable attractors in a network of phase oscillators with three-body interactions. Phys Rev Lett 2011;106:224101.

[25] Millán AP, Torres JJ, Bianconi G. Explosive higher-order kuramoto dynamics on simplicial complexes. Phys Rev Lett 2020;124:218301.

[26] Skardal PS, Arenas A. Higher order interactions in complex networks of phase oscillators promote abrupt synchronization switching. Commun Phys 2020;3:218.

[27] Gambuzza LV, Di Patti F, Gallo L, Lepri S, Romance M, Criado R, et al. Stability of synchronization in simplicial complexes. Nature Commun 2021;12:1255.

[28] Iacopini I, Petri G, Barrat A, Latora V. Simplicial models of social contagion. Nature Commun 2019;10:2485.

[29] de Arruda GF, Petri G, Moreno Y. Social contagion models on hypergraphs. Phys Rev Res 2020;2:023032.

[30] Alvarez-Rodriguez U, Battiston F, de Arruda G, Moreno Y, Perc M, Latora V. Evolutionary dynamics of higher-order interactions in social networks. Nat Hum Behav 2021;5:586.

[31] Civilini A, Sadekar O, Battiston F, Gómez-Gardeñes J, Latora V. Explosive cooperation in social dilemmas on higher-order networks. Phys. Rev. Lett. 2024;132:167401.

[32] Malizia F, Lamata-Otín S, Frasca M, Latora V, Gómez-Gardeñes J. Hyperedge overlap drives explosive collective behaviors in systems with higher-order interactions. 2023, arXiv preprint arXiv:2307.03519.

[33] Roser M, Ortiz-Ospina E, Ritchie H, Hasell J, Appel C, Macdonald B. South Korea: A covid-19 exemplar?. 2020, https://ourworldindata.org/covid-exemplar-south-korea. [Accessed 19 September 2024].

[34] Lau EH, Leung GM. Reply to: Is presymptomatic spread a major contributor to covid-19 transmission? Nature Med 2020;26:1534–5.

[35] Covid-19 pandemic planning scenarios, cdc. 2020, Webpage. https://www.cdc.gov/coronavirus/2019-ncov/hcp/planningscenarios.html, [Accessed 01 July 2020].

[36] Stutt RO, Retkute R, Bradley M, Gilligan CA, Colvin J. A modelling framework to assess the likely effectiveness of facemasks in combination with 'lock-down'in managing the covid-19 pandemic. Proc R Soc A 2020;476:20200376.

[37] To KK-W, Tsang OT-Y, Leung W-S, Tam AR, Wu T-C, Lung DC, et al. Temporal profiles of viral load in posterior oropharyngeal saliva samples and serum antibody responses during infection by sars-cov-2: an observational cohort study. Lancet Infect Dis 2020;20:565–74.

[38] Ozella L, Paolotti D, Lichand G, Rodríguez JP, Haenni S, Phuka J, et al. Using wearable proximity sensors to characterize social contact patterns in a village of rural Malawi. EPJ Data Sci 2021;10:46.

[39] Vanhems P, Barrat A, Cattuto C, Pinton J-F, Khanafer N, Régis C, et al. Estimating potential infection transmission routes in hospital wards using wearable proximity sensors. PLoS One 2013;8:e73970.

[40] Isella L, Stehlé J, Barrat A, Cattuto C, Pinton J-F, Van den Broeck W. What's in a crowd? analysis of face-to-face behavioral networks. J Theoret Biol 2011;271:166–80.

[41] Mastrandrea R, Fournet J, Barrat A. Contact patterns in a high school: A comparison between data collected using wearable sensors, contact diaries and friendship surveys. PLoS One 2015;10:e0136497.

[42] Génois M, Barrat A. Can co-location be used as a proxy for face-to-face contacts? EPJ Data Sci 2018;7:1–18.

[43] Stehlé J, Voirin N, Barrat A, Cattuto C, Isella L, Pinton J-F, et al. High-resolution measurements of face-to-face contact patterns in a primary school. PLoS One 2011;6:e23176.

[44] Salathé M, Kazandjieva M, Lee JW, Levis P, Feldman MW, Jones JH. A high-resolution human contact network for infectious disease transmission. Proc Natl Acad Sci 2010;107:22020–5.

[45] Sapiezynski P, Stopczynski A, Lassen DD, Lehmann S. Interaction data from the copenhagen networks study. Sci Data 2019;6:315.

[46] Gómez-Gardenes J, Lotero L, Taraskin S, Pérez-Reche F. Explosive contagion in networks. Sci Rep 2016;6:19767.

[47] Lamata-Otín S, Gomez-Gardenes J, Soriano D. Pathways to explosive transitions in interacting contagion dynamics. J Phys: Complex 2023.

[48] St-Onge G, Iacopini I, Latora V, Barrat A, Petri G, Allard A, et al. Influential groups for seeding and sustaining nonlinear contagion in heterogeneous hypergraphs. Commun Phys 2022;5:25.

[49] Seufert A, Poignée F, Seufert M, Hoßfeld T. Share and multiply: Modeling communication and generated traffic in private whatsapp groups. IEEE Access 2023;11:25401–14.
[50] Due to finite size and finite connectivity effects, the range of clique sizes appearing in the physical datasets is smaller than in the Seufert et al. dataset, with maximum clique sizes in the range $M \in [7, 28]$. Therefore, we adapt the distribution from the range $m \in [3, 50]$ to the range of cliques in each particular network dataset, i.e., $m \in [3, M]$.
[51] Pastor-Satorras R, Vespignani A. Immunization of complex networks. Phys Rev E 2002;65:036104.
[52] Block P, Hoffman M, Raabe IJ, Dowd JB, Rahal C, Kashyap R, et al. Social network-based distancing strategies to flatten the covid-19 curve in a post-lockdown world. Nat Hum Behav 2020;4:588–96.
[53] Granell C, Gómez S, Arenas A. Dynamical interplay between awareness and epidemic spreading in multiplex networks. Phys Rev Lett 2013;111:128701.
[54] Granell C, Gómez S, Arenas A. Competing spreading processes on multiplex networks: awareness and epidemics. Phys Rev E 2014;90:012808.
[55] Nie Y, Zhong M, Li R, Zhao D, Peng H, Zhong X, et al. Digital contact tracing on hypergraphs. Chaos 2023;33.
[56] Rosenfeld A, Sina S, Sarne D, Avidov O, Kraus S. Whatsapp usage patterns and prediction of demographic characteristics without access to message content. Demogr Res 2018;39:647–70.
[57] Malizia F, Gallo L, Frasca M, Latora V, Russo G. A pair-based approximation for simplicial contagion. 2023, arXiv preprint arXiv:2307.10151.
[58] Kim J, Lee D-S, Goh K-I. Contagion dynamics on hypergraphs with nested hyperedges. Phys Rev E 2023;108:034313.
[59] Landry NW, Restrepo JG. The effect of heterogeneity on hypergraph contagion models. Chaos 2020;30.
[60] Schwind A, Seufert M. Whatsanalyzer: A tool for collecting and analyzing whatsapp mobile messaging communication data. In: 2018 30th International teletraffic congress (ITC 30), vol. 1, IEEE; 2018, p. 85–8.
[61] Seufert A, Poignée F, Hoßfeld T, Seufert M. Pandemic in the digital age: analyzing whatsapp communication behavior before, during, and after the covid-19 lockdown. Humanit Soc Sci Commun 2022;9.
[62] Machado C, Kira B, Narayanan V, Kollanyi B, Howard P. A study of misinformation in whatsapp groups with a focus on the brazilian presidential elections. In: Companion proceedings of the 2019 world wide web conference. 2019, p. 1013–9.
[63] Lamata-Otín S, Reyna-Lara A, Soriano-Paños D, Latora V, Gómez-Gardeñes J. Collapse transition in epidemic spreading subject to detection with limited resources. Phys Rev E 2023;108:024305.
[64] Williams BJ, St-Onge G, Hébert-Dufresne L. Localization, epidemic transitions, and unpredictability of multistrain epidemics with an underlying genotype network. PLoS Comput Biol 2021;17:e1008606.
[65] Zhang X, Ruan Z, Zheng M, Zhou J, Boccaletti S, Barzel B. Epidemic spreading under mutually independent intra-and inter-host pathogen evolution. Nature Commun 2022;13:6218.
[66] Mancastroppa M, Iacopini I, Petri G, Barrat A. The structural evolution of temporal hypergraphs through the lens of hyper-cores. 2024, arXiv preprint arXiv:2402.06485.
[67] Gallo L, Lacasa L, Latora V, Battiston F. Higher-order correlations reveal complex memory in temporal hypergraphs. Nature Commun 2024;15(1):4754.